J Therm Anal Calorim (2012) 108:817–823
DOI 10.1007/s10973-012-2196-7

Phase equilibria of the Dy–Al–Si system at 500 °C

Anna Maria Cardinale · Daniele Macciò · Adriana Saccone

MEDICTA2011 Conference Special Chapter

Abstract The isothermal section at 500 °C of the Dy–Al–Si system was studied in the whole concentration range. The alloys were characterized by X-ray powder diffraction, scanning electron microscopy and electron micro-probe analysis. A few samples were analysed by differential thermal analysis. The following intermetallic compounds, some of them showing variable composition, were found: $DyAl_2Si_2$ (τ_1), hP5-$CaAl_2O_2$ structure type, $Dy_2Al_3Si_2$ (τ_2) mS14-$Y_2Al_3Si_2$ structure type, $Dy_2Al_{1+x}Si_{2-x}$ (τ_3), $0 \leq x \leq 0.25$, oI10-W_2CoB_2 structure type and Dy_6Al_3Si (τ_4), tI80-Tb_6Al_3Si structure type. A number of binary phases dissolve the third element forming ternary solid solutions: $Dy(Al_{1-x}Si_x)_3$, $0 \leq x \leq 0.5$, hP16-Ni_3Ti structure type, $Dy(Al_xSi_{1-x})_2$, $0 \leq x \leq 0.1$, oI12-$GdSi_2$ structure type, $Dy(Al_xSi_{1-x})_{1.67}$, $0 \leq x \leq 0.2$, oI12-$GdSi_2$ structure type, $DyAl_xSi_{1-x}$, $0 \leq x \leq 0.2$, oC8-CrB, and $Dy_5(Al_xSi_{1-x})_3$, $0 \leq x \leq 0.3$, hP16-Mn_5Si_3 structure type. The melting point of Dy_6Al_3Si was determined.

Keywords Phase diagrams · Intermetallic compounds · Aluminium alloys · Rare earth alloys · Silicon alloys

Introduction

The experimental investigation of the Dy–Al–Si system is part of an ongoing research project carried out by our group with the aim to clarify the phase equilibria of ternary systems of aluminium and silicon with rare earth metals.

A. M. Cardinale (✉) · D. Macciò · A. Saccone
Dipartimento di Chimica e Chimica Industriale, Università di Genova, Via Dodecaneso, 31-16146 Genoa, Italy
e-mail: cardinal@chimica.unige.it

The Al–Si alloys are important and widely used casting alloys for their excellent properties, such as low thermal expansion coefficient, good casting performance, good weldability, high wear resistance, high corrosion resistance and high temperature strength [1, 2]. The addition of a third element, in particular rare earth metals, can improve these technological properties [3].

A few R–Al–Si isothermal sections (R = rare earth metals), even though only partially investigated, have been reported in the literature. They are: La–Al–Si (0–33 at% La) [4], Ce–Al–Si [5], Pr–Al–Si (0–33 at% Pr) [6], Gd–Al–Si [7], Ho–Al–Si [8], Er–Al–Si [9] and Y–Al–Si [10].

Recently, we showed the results obtained in the study of the Nd–Al–Si phase diagram [11]. In this study, we report the isothermal section at 500 °C of the Dy–Al–Si system.

No information on the Dy–Al–Si phase diagram is available in the literature. All binary subsystems Al–Si, Dy–Al and Dy–Si can be found in Okamoto's collection of binary phase diagrams [12].

Table 1 shows the stoichiometry and the crystal structure of the relevant binary and ternary compounds reported in literature.

Experimental procedure

The elements used as starting materials were neodymium 99.9 mass% purity, aluminium 99.999 mass% purity and silicon 99.99 mass% purity (all supplied by Newmet Koch, Waltham Abbey, England). About 50 ternary alloys were prepared by induction melting the stoichiometric amounts of the constituent metals enclosed in small arc-sealed tantalum crucibles (for low content of aluminium) or by arc melting (for low content of dysprosium). For homogeneity, the samples were re-melted

Table 1 Crystallographic data of the binary boundary and ternary phases of the Dy–Al, Dy–Si, Al–Si and Dy–Al–Si systems

Phase	Crystal structure-prototype	Remarks	Refs.
βDy	cI2-W	$T < 1{,}657$ °C	[17]
αDy	hP2-Mg	1,657 °C $< T >$ 1,685 °C	[17]
Al	cF4-Cu		[17]
Si	cF8-$C_{diamond}$		[17]
$\beta DyAl_3$	hR60-$HoAl_3$	$T > 1{,}005$ °C	[18]
$\alpha DyAl_3$	hP16-$TiNi_3$	$T < 1{,}005$ °C	[19]
$DyAl_2$	cF24-$MgCu_2$		[20]
DyAl	oP16-AlEr		[20]
Dy_3Al_2	tP20-Al_2Zr_3		[20]
Dy_2Al	oP12-Co_2Si		[20]
Dy_5Si_3	hP16-Mn_5Si_3		[21]
Dy_5Si_4	oP36-Sm_5Ge_4,		[22]
$\beta DySi_{1-x}$	oP8-FeB	800 °C $< T <$ 1,890 °C	[23]
αDySi	oC8-CrB	$T < 800$ °C	[23]
Dy_3Si_4	oS24-Ho_3Si_4		[24]
$\beta DySi_{1.67}$	hP3-AlB_2	760 °C $< T <$ 1,635 °C	[25]
$\alpha DySi_{1.67}$	oI12-$GdSi_2$	$T < 760$ °C	[17]
$\beta DySi_2$	tI12-$ThSi_2$	540 °C $< T <$ 1,430 °C	[26]
$\alpha DySi_2$	oI12-$GdSi_2$	$T < 540$ °C	[17]
$DyAl_2Si_2$	(hP5-$CaAl_2O_2$)		[27]
$Dy_2Al_3Si_2$	(mS14-$Y_2Al_3Si_2$)		[28]
Dy_6Al_3Si	(tI80-Tb_6Al_3Si)		[29]
DyAlSi	oS12-YAlGe	$T = 600$ °C	[15]
	tI10-$\alpha ThSi_2$	$T = 700$ °C	[16]

several times under a stream of pure argon. The alloys enclosed in alumina crucibles were then sealed in silica ampoules under argon and annealed in a resistance furnace at 500 °C for 360 h. After quenching in cold water the samples were characterized by means of light optical microscopy (LOM), scanning electron microscopy (SEM) and electron probe microanalysis based on energy dispersive X-ray spectroscopy (EDXS), to investigate microstructure and to measure phase composition. Smooth surfaces of specimens for microscopic observation were prepared by using SiC papers and diamond pastes down to 1-μm grain size. For the quantitative analysis an acceleration voltage of 20 kV was applied for 50 s, and a cobalt standard was used for calibration. The software packaging Inca Energy (Oxford Instruments, Analytical Ltd., Bucks, UK) was employed to process X-ray spectra. To determine crystal structures and calculate lattice parameters X-ray diffraction analysis (PXRD) was performed on powdered samples by using a vertical diffractometer X'Pert MPD (Philips, Almelo, The Netherlands).

For a few alloys differential thermal analysis (DTA) was carried out, both on heating and on cooling, at rate 10 K min^{-1} by using samples enclosed in sealed tantalum crucibles. The instrument used was a model 404S Netzsch apparatus (Selb, Germany).

More details about the operating conditions are described, for instance, in Ref. [13].

Results and discussion

Figure 1a depicts the compositions of the alloys investigated. The isothermal section at 500 °C, drawn on the basis of the results achieved, is shown in Fig. 1b.

The results obtained for several alloys from the analysis by SEM/EDXS and X-ray powder diffraction are listed in Table 2. Photomicrographs of significant samples are shown in Fig. 2a–d.

All the Dy–Al and Dy–Si binary compounds given in the literature were confirmed with the exception of Dy_3Si_4. A few binary phases of the Dy–Si boundary system dissolve an appreciable amount of the third element (Al), forming ternary solid solutions whose homogeneity ranges are at a constant Dy content: $Dy(Al_xSi_{1-x})_2$, $0 \le x \le 0.1$,

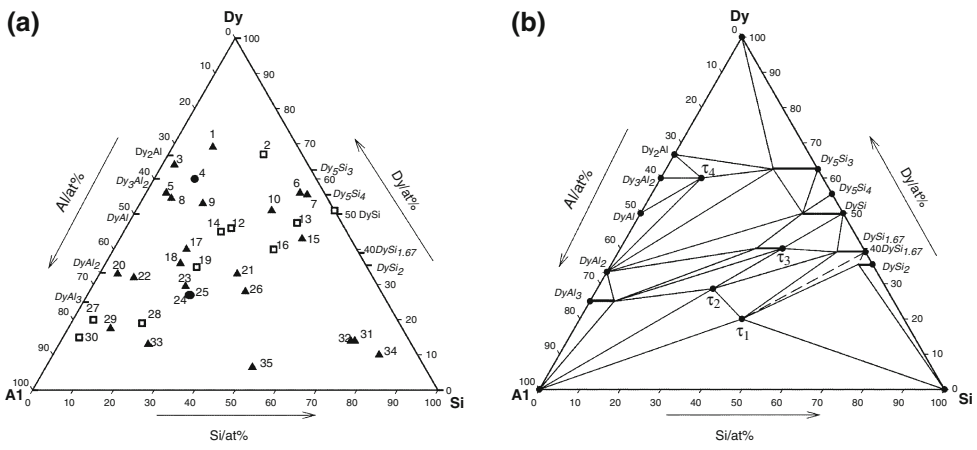

Fig. 1 Dy–Al–Si system. **a** Gross composition of the analyzed alloys (*filled triangle* three phase samples; *open square* two-phase samples; *filled circle* single-phase samples). The results of the characterization of the coded samples are shown in Table 1. **b** Isothermal section at 500 °C. Equilibria indicated with *dashed lines* require confirmation

Table 2 Selected Dy–Al–Si samples annealed at 500 °C: SEM–EDXS and PXRD results

Code	Nominal composition/at%	Phases analysis	Crystal structure	EDXS results		Lattice parameters/nm		
				Dy, Al, Si/at%	∑mass%	*a*	*b*	*c*, *β*/°
1	$Dy_{69}Al_{21}Si_{10}$	αDy	hP2-Mg	~100.0, 0.0, 0.0	98	0.3612(8)		0.5601(7)
		Dy_2Al	oP12-Co_2Si	67.0, 33.0, 0.0	98	0.6507(4)	0.5084(5)	0.9382(4)
		$Dy_5(Al_xSi_{1-x})_3$	hP16-Mn_5Si_3	63.0, 13.0, 24.0	97	0.8507(4)		0.6307(3)
2	$Dy_{67}Al_{9.5}Si_{23.5}$	αDy	hP2-Mg	95.0, 5.0, 0.0	103	0.3495(1)		0.5493(8)
		$Dy_5(Al_xSi_{1-x})_3$	hP16-Mn_5Si_3	61.0, 5.0, 33.0	101	0.8394(3)		0.6267(5)
3	$Dy_{64}Al_{33}Si_3$	Dy_3Al_2	tP20-Al_2Zr_3	62.0, 38.0,0.0	99	0.8203(2)		0.7531(3)
		Dy_2Al	oP12-Co_2Si	67.0, 33.0, 0.0	98	0.6521(5)	0.5072(3)	0.9374(6)
		τ_4	tI80-Tb_6Al_3Si	61.5, 30.0, 8.5	99	1.1550(4)		1.4960(8)
4	$Dy_{60}Al_{30}Si_{10}$	τ_4	tI80-Tb_6Al_3Si	59.0, 28.8, 12.2	102	1.1530(2)		1.5033(4)
5	$Dy_{56.0}Al_{39.0}Si_5$	Dy_3Al_2	tP20-Al_2Zr_3	62.0, 38.0, 0.0	97	0.8168(5)	1.1362(7)	0.7515(8)
		τ_4	tI80-Tb_6Al_3Si	59.5, 25.5, 15.0	99	1.1542(4)		1.4941(6)
		Dy Al	oP16-ErAl	52.0, 48.0, 0.0	98	0.5824(6)		0.5601(3)
6	$Dy_{56}Al_6Si_{38}$	$Dy_5(Al_xSi_{1-x})_3$	hP16-Mn_5Si_3	61.5, 1.5, 37.0	101	0.8366(4)		0.6295(10)
		Dy_5Si_4	oP36-Sm_5Ge_4	55.0, 1.0, 44.0	100	0.7358(4)	1.4505(2)	0.7649(3)
		$DySi_{1-x}Al_x$	oC8-CrB	49.5, 13.5, 37.0	100	0.4269(5)	1.0536(11)	0.3813(2)
7	$Dy_{55.5}Al_{4.5}Si_{40}$	$Dy_5(Al_xSi_{1-x})_3$	hP16-Mn_5Si_3	61.5, ~0.0, 38.5	98	0.8353(4)		0.6274(5)
		Dy_5Si_4	oP36-Sm_5Ge_4	55.0, 0.0, 45.0	99	0.7371(3)	1.4518(8)	0.7676(3)
		$DyAl_xSi_{1-x}$	oC8-CrB	50.0, 12.0,38.0	100	0.4251(1)	1.0511(3)	0.3829(9)
8	$Dy_{53.5}Al_{38.5}Si_{8.0}$	DyAl	oP16-ErAl	50.0, 50.0, 0.0	102	0.5803(3)	1.1359(11)	0.5589(3)
		τ_4	tI80-Tb_6Al_3Si	55.0, 20.5, 24.5	101	1.1499(6)		1.505688)
		Dy Al_2	cF24-Cu_2Mg	34.5, 65.5, 0.0	101	0.7831(2)		
9	$Dy_{52.0}Al_{31.5}Si_{16.5}$	$Dy_5(Al_xSi_{1-x})_3$	hP16-Mn_5Si_3	62.5, 5.0, 32.5	99	0.8388(3)		0.6314(3)
		τ_4	tI80-Tb_6Al_3Si	59.5, 26.0, 14.5	99	1.1530(2)		1.4965(6)
		$DyAl_2$	cF24-Cu_2Mg	34.0, 66.0, 0.0	100	0.7832(1)		
10	$Dy_{51.0}Al_{15.5}Si_{33.5}$	$DyAl_xSi_{1-x}$	oC8-CrB	51.0, 41.0, 8.0	101	0.4266(4)	1.0652(2)	0.3832(3)
		$Dy_5(Al_xSi_{1-x})_3$ Dy	hP16-Mn_5Si_3	60.0, 14.0, 26.0	100	0.8374(3)		0.6288(8)
		Al_2	cF24-Cu_2Mg	36.0, 64.0, 0.0	100	0.7829(1)		
11	$Dy_{51.0}Si_{49.0}$	Dy_5Si_4	oP36-Sm_5Ge_4	54.0, 0.0, 46.0	100	0.7373(4)	1.4536(3)	0.7675(3)
		DySi	oC8-CrB	50.5, 0.0, 49.5	99	0.3972(6)	1.0257(4)	0.3658(5)
12	$Dy_{46.0}Al_{28.0}Si_{26.0}$	$DyAl_xSi_{1-x}$	oC8-CrB	50.0, 11.0, 39.0	100	0.4270(2)	1.0695(2)	0.3853(3)
See Fig. 2a		$DyAl_2$	cF24-Cu_2Mg	35.0, 65.0, 0.0	101	0.7826(4)		
13	$Dy_{47.5}Al_{11.0}Si_{41.5}$	τ_3	oI10-W_2CoB_2	40.0, 26.0, 34.0	99	0.8578	0.5730	0.4009
		$DyAl_xSi_{1-x}$	oC8-CrB	50.0, 3.5, 46.5	100	0.4233(3)	1.0559(5)	0.3844(7)
14	$Dy_{45.0}Al_{31.0}Si_{24.0}$	$DyAl_xSi_{1-x}$	oC8-CrB	50.0, 12.5, 37.5	98	0.4230(4)	1.0634(6)	0.3803(2)
		Dy Al_2	cF24-Cu_2Mg	33.5, 66.5, 0.0	98	0.7830(1)		
15	$Dy_{43.0}Al_{12.0}Si_{45.0}$	τ_3	oI10-W_2CoB_2	40.5, 18.5, 41.0	100	4.0384(1)	5.7251(2)	8.6269(3)
		$DyAl_xSi_{1-x}$	oC8-CrB	50.5, 1.0, 48.5	101	0.4249(2)	1.0502(5)	0.3821(2)
		$Dy(Al_xSi_{1-x})_{1.67}$	oI12-Gd_2Si	36.5, 3.0, 60.5	98	0.3964(3))	0.4035(7)	1.3227(4)
16	$Dy_{40.0}Al_{20.5}Si_{39.5}$	τ_3	oI10-W_2CoB_2	41.0, 20.0, 39.0	97	0.8665(4)	0.5731(5)	0.4053(3)
		$DyAl_xSi_{1-x}$	oC8-CrB	50.5, 1.5, 48.0	98	0.3363(8)	0.8344(4)	0.3930(6)
17	$Dy_{40.0}Al_{42.0}Si_{18.0}$	$DyAl_xSi_{1-x}$	oC8-CrB	51.0, 10.0, 39.0	97	0.4266(5)	1.0582(4)	0.3875(4)
See Fig. 2b		τ_3	oI10-W_2CoB	40.5, 25.5, 34.0	96	0.8568(7)	0.5790(5)	0.3960(5)
		$DyAl_2$	cF24-Cu_2Mg	34.0, 64.0, 2.0	99	0.7814(1)		
18	$Dy_{37.0}Al_{45.0}Si_{18.0}$	τ_3	oI10-W_2CoB_2	40.5, 26.5, 33.0	99	0.4008(2)	0.5745(5)	0.8553(3)
		$DyAl_2$	cF24-Cu_2Mg	34.0, 63.0, 3.0	101	0.7806(1)		
		$DyAl_{3-x}Si_x$	hP16-$TiNi_3$	28.5, 65.5, 6.0	101	0.608984)		0.9699(3)

Table 2 continued

Code	Nominal composition/at%	Phases analysis	Crystal structure	EDXS results		Lattice parameters/nm		
				Dy, Al, Si/at%	∑mass%	*a*	*b*	*c*, *β*/°
19	$Dy_{35.0}Al_{42.0}Si_{23.0}$	$DyAl_{3-x}Si_x$	hP16-$TiNi_3$	25.0, 68.0, 7.0	99	0.6158(8)		0.9486(10)
		τ_3	oI10-W_2CoB_2	40.0, 25.5, 34.5	98	0.8561(10)	0.5697(9)	0.4005(6)
20	$Dy_{33.0}Al_{62.5}Si_{4.5}$	$DyAl_2$	cF24-Cu_2Mg	34.0, 66.0, 0.0	103	0.7804(2)		
		$DyAl_{3-x}Si_x$	hP16-$TiNi_3$	26.0,67.5, 6.5	101	0.6244(4)		0.9528(3)
		τ_3	oI10-W_2CoB_2	39.0, 26.0, 35.0	101	0.8691(3)	0.5697(8)	0.4035(11)
21	$Dy_{33.0}Al_{33.0}Si_{34.0}$	τ_3	oI10-W_2CoB_2	41.0, 18.0, 41.0	99	0.3993(3)	0.57348(3	0.8563(7
		$Dy(Al_xSi_{1-x})_{1.67}$	oI12-Gd_2Si	37.0, 7.0, 56.0	99	0.3915(6)	0.4025(6)	1.3356(12)
		τ_2	mS14-$Y_2Al_3Si_2$	29.5, 42.0 28.5	100	1.0124(3)	0.4028(1)	0.6577(7)
								$\beta = 100.95$
22	$Dy_{32.0}Al_{59.0}Si_{9.0}$	τ_3	oI10-W_2CoB_2	40.0, 25.0, 35.0	99	0.4144(8)	0.5706	0.8572(6)
See Fig. 2c		$DyAl_{3-x}Si_x$	hP16- Ti Ni_3	25.0, 67.5, 7.5	98	0.6147(5)		0.9575(12)
		$DyAl_2$	cF24-Cu_2Mg	33.5, 65.0, 1.5	99	0.7808(1)		
23	$Dy_{29.5}Al_{47.5}Si_{23.0}$	τ_3	oI10-W_2CoB_2	41.0, 20.5, 38.0	100	0.4032(5)	0.5746(6)	0.8510(6)
		$DyAl_{3-x}Si_x$	hP16-Ti Ni_3	26.0, 66.0, 8.0	100	0.6142(2)		0.9537(8)
		τ_2	mS14-$Y_2Al_3Si_2$	29.5, 42.5, 28.0	102	1.0149(3)	0.4025(2)	0.6573(3)
								$\beta = 100.93$
24	$Dy_{27.0}Al_{48.0}Si_{25.0}$	τ_2	mS14-$Y_2Al_3Si_2$	29.0, 44.0, 27.0	99	1.013(8)	0.403(2)	0.6574(9)
								$\beta = 100.83(2)$
25	$Dy_{27.0}Al_{47.5}Si_{25.5}$	τ_2	mS14-$Y_2Al_3Si_2$	29.5, 43.1, 27.4	100	1.0134(6)	0.4024(2)	0.6577(4)
								$\beta = 100.93$
26	$Dy_{28}Al_{33.5}Si_{38.5}$	$Dy(Al_xSi_{1-x})_{1.67}$	oI12-Gd_2Si	36.0, 6.5, 57.5	98	0.3949(5)	0.4026(3)	1.3344(6)
		τ_1	hP5-$CaLa_2O_2$	22.0, 40.0, 38.0	98	0.4174(3)		0.6545(6)
		τ_2	mS14-$Y_2Al_3Si_2$	28.5, 42.0, 22.5	100	1.0130(3)	0.4025(1)	0.6574(2)
								$\beta = 104.04(0)$
27	$Dy_{20.0}Al_{75.0}Si_{5.0}$	$DyAl_{3-x}Si_x$	hP16-$TiNi_3$	24.5, 70.5, 5.0	99	0.6093(6)		0.9518(9)
See Fig. 2d		Al	cF4-Cu	0.0, ~100, 0.0	100	0.4045(1)		
28	$Dy_{19.0}Al_{63.5}Si_{17.5}$	τ_2	mS14-$Y_2Al_3Si_2$	27.3 48.0, 24.7	101	1.0029(3)	0.4033(3)	0.6487(3)
		Al	cF4-Cu	0.0, ~100.0, 0.0	100			$\beta = 99.53(0))$
29	$Dy_{17.5}Al_{72.0}Si_{10.5}$	$DyAl_{3-x}Si_x$	hP16-$TiNi_3$	26.5, 67.5, 6.0	97	0.6090(3)		0.9467(10)
		τ_2	mS14-$Y_2Al_3Si_2$	30.0, 42.5, 27.5	97	1.0128(6)	0.4026(2)	0.6577(7)
		Al	cF4-Cu	0.0, ~100, 0.0	98	0.4078(8)		$\beta = 100.99(1)$
30	$Dy_{15.0}Al_{81.0}Si_{4.0}$	$DyAl_{3-x}Si_x$	hP16-$TiNi_3$	24.5, 70.5, 5.0	101	0.6093(6)		0.9518(9)
		Al	cF4-Cu	0.0, ~100.0, 0.0	100	0.4045(1)		
31	$Dy_{14.0}Al_{13.5}Si_{72.5}$	$Dy(Al_xSi_{1-x})_2$	oI12-$GdSi_2$	37.0, 3.5, 59.5	102	0.4035(3)	0.3959(3)	1.3321(9)
		τ_1	hP5-$CaLa_2O_2$	21.0, 40.0, 39.0	99	0.4182(7)		0.6559(11)
		Si	cF8-C(diamond)	0.0, 0.0, ~100.0	99	0.5498(9)		
32	$Dy_{14.0}Al_{14.5}Si_{71.5}$	τ_1	hP5-$CaLa_2O_2$	20.0, 39.0, 41.0	98	0.4179(2)		6.5490(3)
		$Dy(Al_xSi_{1-x})_2$	oI12-GdSi	35.0, 3.0, 62.0	98	0.4055(2)	0.3937(4)	1.3332(2)
		Si	cF8-C(diamond)	0.0, 0.0, ~100.0	99	0.5107(1)		
33	$Dy_{12.0}Al_{66.0}Si_{22.0}$	τ_2	mS14-$Y_2Al_3Si_2$	28.0, 43.0, 29.0	98	0.9905(7)	0.3991(8)	0.6650(4)
		τ_1	hP5-$CaLa_2O_2$	20.0, 40.0, 40.0	98	0.4182(6)		$\beta = 103.17$
		Al	cF4-Cu	0.0, ~100.0, 0.0	97	0.4048(4)		0.6558(4)
34	$Dy_{10.0}Al_{9.0}Si_{81.0}$	$Dy(Al_xSi_{1-x})_2$	oI12-$GdSi_2$	34.5, 4.0, 61.5	99	0.4046(3)	0.3943(3)	1.3321(9)
		τ_1	hP5-$CaLa_2O_2$	19.5, 40.2, 40.3	101	0.4542(1)		0.7133(2)
		Si	cF8-C(diamond)	0.0, 0.0, ~100.0	100	0.5440(5)		

Table 2 continued

Code	Nominal composition/at%	Phases analysis	Crystal structure	EDXS results		Lattice parameters/nm		
				Dy, Al, Si/at%	∑mass%	*a*	*b*	*c*, *β*/°
35	$Dy_{6.5}Al_{42.5}Si_{51.0}$	Al	cF4-Cu	0.0, ~100.0, 0.0	98	0.4147(3)		
		Si	cF8-C(diamond)	0.0, 0.0, ~100.0	99	0.5432(4)		
		τ_1	hP5-$CaLa_2O_2$	20.0, 40.0, 40.0	98	0.4181(1)		0.6558(2)

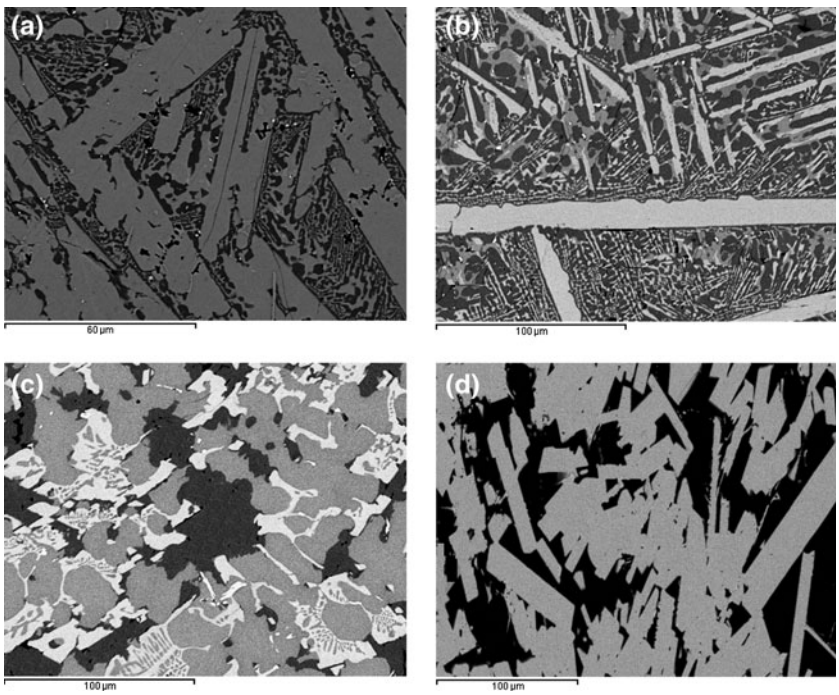

Fig. 2 Back scattered electrons (BSE) images of some selected Dy–Al–Si samples. **a** sample N. 12: *white phase* ($DyAl_xSi_{1-x}$) and *grey phase* ($DyAl_2$). **b** sample N. 17: *white phase* ($DyAl_{1-x}Si_x$), *light grey phase* (τ_3), *dark grey phase* ($DyAl_2$). **c** Sample N. 22: *white phase* (τ_3), *grey phase* ($DyAl_2$), *black phase* ($DyAl_{3-x}Si_x$). **d** Sample N. 27: *white phase* ($DyAl_{3-x}Si_x$), *black phase* (Al)

$Dy(Al_xSi_{1-x})_{1.67}$, $0 \le x \le 0.2$, $DyAl_xSi_{1-x}$, $0 \le x \le 0.2$ and $Dy_5(Al_xSi_{1-x})_3$, $0 \le x \le 0.3$. These homogeneity ranges were determined by SEM/EDXS quantitative analysis and confirmed by the variation of the lattice parameters. A Si/Al substitution mechanism can be suggested for these solid solutions.

As for the other binary boundary phases only the $DyAl_3$ phase dissolves appreciably the third element (Si) forming the $Dy(Al_{1-x}Si_x)_3$ solid solution ($0 \le x \le 0.5$).

Solid solutions based on binary phases extending less that 1% in the ternary field were not taken into account.

A number of ternary intermetallic compounds were found. The $DyAl_2Si_2$ (τ_1), $Dy_2Al_3Si_2$ (τ_2) and Dy_6Al_3Si (τ_4) phases were confirmed. They crystallize in the hexagonal hP5-$CaAl_2O_2$ structure type, monoclinic mS14-$Y_2Al_3Si_2$ structure type and tetragonal tI80-Tb_6Al_3Si structure type, respectively.

The $Dy_2Al_{1+x}Si_{2-x}$, $0 \le x \le 0.25$ (τ_3), compound was not previously reported in the literature. The X-ray

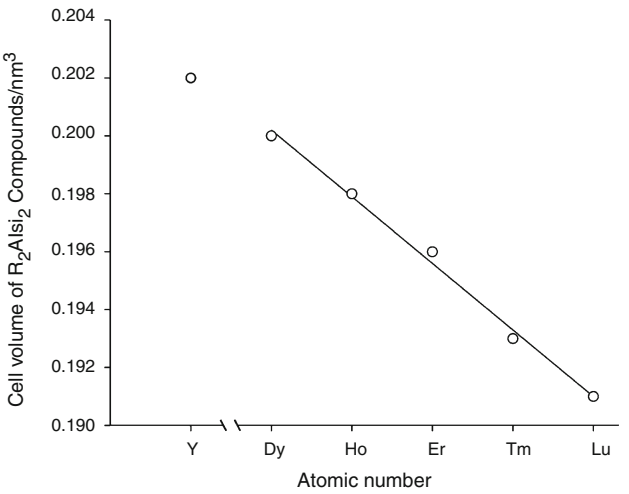

Fig. 3 Trend of the cell volume of the R_2AlSi_2 compounds plotted against the atomic number of the rare earths. For comparison the yttrium value has been added (due its atomic size, yttrium behaves as the heavy rare earths)

Table 3 Ternary Dy–Al–Si intermediate compounds: crystallographic data

Compound	Crystal structure	Lattice parameters/nm			Refs.
		a	*b*	*c*, *β*/°	
$DyAl_2Si_2$ (τ_1)	hP5-$CaAl_2O_2$	0.4185(1)		0.6569(4)	[27]
		0.4182(7)		0.6559(11)	This work
$Dy_2Al_3Si_2$ (τ_2)	mS14-$Y_2Al_3Si_2$	1.0133(3)	0.4030(9)	0.6608(1), $\beta = 100.83(2)$	[28]
		1.0130(8)	0.4030(2)	0.6574(9),$\beta = 100.83(2)$	This work
$Dy_2Al_{1+x}Si_{2-x}$ (τ_3) $0 \leq x \leq 0.25$	oI10-W_2CoB_2	0.8665(4)	0.5731(5)	0.4053(3)	This work
Dy_6Al_3Si (τ_4)	tI80-Tb_6Al_3Si	1.1535(8)		1.497(2)	[29]
		1.1530(2)		1.5033(4)	This work

diffraction analysis carried out on several samples containing this phase show that it is isostructural with R_2AlSi_2 (R = Ho, Er, Tm, Lu, Y) [14]. The Dy_2AlSi_2 compound crystallizes orthorhombic, oI10-W_2CoB_2 structure type. As can be seen from Fig. 3, the cell volume of these isotypic compounds gradually decreases with decreasing the atomic radius of the rare earth involved. A homogeneity range at a constant Dy content (40 at%) was detected for τ_3 extending towards Al-rich compositions with respect to the stoichiometric formula Dy_2AlSi_2.

The equiatomic phase DyAlSi reported in the literature at 600 °C [15] and 700 °C [16] was not confirmed in the isothermal section investigated.

Table 3 collects the lattice parameters of the ternary compounds found in the Dy–Al–Si system.

DTA was carried out on a single-phase sample having the Dy_6Al_3Si (τ_4) composition. The phase melts congruently at 1,030 °C; this melting mechanism was also confirmed by the micrographic appearance of the alloy after DTA.

Conclusions

Phase relations in the Dy–Al–Si system, at 500 °C were derived by SEM, EDXS and PXRD analysis. Four ternary compounds take part in the phase equilibria: three already known ternary compounds $DyAl_2Si_2$ (τ_1), $Dy_2Al_3Si_2$ (τ_2) and Dy_6Al_3Si (τ_4) were confirmed and one new ternary phase $Dy_2Al_{1+x}Si_{2-x}$ (τ_3) existing in the $0 \leq x \leq 0.25$ range and isostructural with R_2AlSi_2 (R = Ho, Er, Tm, Lu, Y) was detected.

The isothermal section of the Dy–Al–Si system can be fruitfully compared with the previously studied Nd–Al–Si isothermal section, both systems referring to the alloying behaviour of rare earths with Al and Si, but highlighting the different reactivity of a light rare earth (Nd) with respect to a heavy rare earth (Dy).

The Nd–Al–Si and Dy–Al–Si isothermal sections are characterized by intermediate phases having in general different stoichiometries; these phases, in analogy with the phases found in other R–Al–Si systems are localized in the 20–60 at% rare earth range. A decreasing of the number of the intermediate phases seems to characterize these systems on passing from the light to the heavy rare earths.

Phase equilibria of other R–Al–Si ternary systems are currently under investigation.

References

1. Slattery BE, Perry T, Edrisy A. Microstructural evolution of a eutectic Al–Si engine subjected to severe running conditions. Mater Sci Eng A. 2009;512:76–81.
2. Miller WS, Zhuang L, Bottema J, Wittebrood AJ, De Smet P, Haszler A, Vieregge A. Recent development in aluminium alloys for the automotive industry. Mater Sci Eng A. 2000;280:37–49.
3. Zhu M, Jian Z, Yao L, Liu C, Yang G, Zhou Y. Effect of mischmetal modification treatment on the microstructure, tensile properties, and fracture behavior of Al–7.0% Si–0.3% Mg foundry aluminum alloys. J Mater Sci. 2011;46:2685–94.
4. Murav'eva AO. The systems La–Al–Si and La–Al–Sb in the region 0–33.3 at% La. Vestn Lviv Univ Ser Khim. 1971;12:8–9.
5. Flandorfer H, Kaczorowski D, Gröbner J, Rogl P, Godart C, Kostikas A. The systems Ce–Al–(Si, Ge): phase equilibria and physical properties. J Solid State Chem. 1998;137:191–205.
6. Nakonechna N, Lyaskovska N, Romaniv O, Starodub P, Gladyshevskii E. Pr–Al–Si phase diagram (0–0.33 at.fract. Pr) and crystal structure of the compounds. Visn Lviv Univ Ser Khim. 2001;40:61–7.
7. Zarechnyuk OS, Yanson TI, Murav'eva AA. The systems Gd–Al–Si, Gd–Al–Ge in the range 0–0.33 of gadolinium. Visn Lviv Univ Ser Khim. 1981;23:64–7.
8. Zhuang YH, Li JQ, Zeng LM. The isothermal section (500 °C) of the phase diagram of the Al–Ho–Si ternary system. J Less Common Met. 1990;157:47–53.
9. Pukas S, Lasocha W, Gladyshevskii R. Phase equilibria in the Er–Al–Si system at 873 K. CALPHAD. 2009;33:23–6.
10. Murav'eva AO, Zarechnyuk OS, Gladyshevskii EI. The systems Y–Al–Si(Ge, Sb) in the range 0–33.3 at% Y. Izv Akad Nauk SSSR Neorg Mater. 1971;1(7):38.
11. Cardinale AM, Macciò D, Delfino S, Saccone A. Experimental investigation of the Nd–Al–Si system. J Therm Anal Calorim. 2011;103:103–9.

12. Okamoto H. Desk handbook: phase diagrams for binary alloys. Materials Park, OH: ASM International; 2000.
13. Saccone A, Cardinale AM, Delfino S, Ferro R. Phase equilibria in the rare erath metals (R)-rich regions in the R–Al systems (R = La, Ce, Pr, Nd). Z Metallkd. 1996;87:82–7.
14. Kranenberg C, Mewis A. Synthesis and crysta structures of $Ln_2Al_3Si_2$ and Ln_2AlSi_2 (Ln: Y, Tb–Lu). Z Anorg Allg Chem. 2000;626:1448–53.
15. Pukas S, Lutsyshyn Y, Manyako M, Gladyshevskii E. Crystal structures of the RAlSi and RAlGe compounds. J Alloys Compd. 2004;367:162–6.
16. He W, Zhang J, Zeng L. New structure of the ternary compound DyAlSi. J Alloys Compd. 2006;424:105–7.
17. Villars P, Cenzual K. Pearson's crystal data–crystal structure database for inorganic compounds, Release 2010/11. Materials Park, OH, USA: ASM International.
18. Van Vucht JHN, Buschow KHJ. On the binary aluminium-rich compounds of the rare-earth elements. Philips Res Rep. 1964;19: 319–22.
19. Baenziger NC, Hegenbarth JJ. Gadolinium and dysprosium intermetallic phases. III. The structures of Gd_3Al_2, Dy_3Al_2, Gd_5Ge_3, Dy_5Ge_3 and $DyAl_3$. Acta Crystallogr. 1964;17:620–1.
20. Saccone A, Cardinale AM, Delfino S, Ferro R. Gd–Al and Dy–Al systems: phase equilibria in the 0–66.7 at% Al composition range. Z. Metallkd. 2000;91:17–23.
21. Mayer I, Felner I. High-temperature X-ray study of rare-earth silicides. J Less Common Met. 1972;29:25–31.
22. Holtzberg F, Gambino RJ, McGuire TR. New ferromagnetic 5:4 compounds in the rare earth silicon and germanium systems. J Phys Chem Solids. 1967;28:2283–9.
23. Hohnke D, Parthè E. AB Compounds with Sc, Y and rare earth metals. II. FeB and CrB type structures of monosilicides and germanides. Acta Crystallogr. 1966;20:572–82.
24. Roger J, Guizouarn T, Hiebl K, Halet JF, Guérin R. Structural chemistry and physical properties of the rare earth silicide Dy_3Si_4. J Alloys Compd. 2005;394:28–34.
25. Iandelli A, Palenzona A, Olcese GL. Valence fluctuations of ytterbium in silicon-rich compounds. J Less Common Met. 1979;64: 213–20.
26. Perri JA, Banks E, Post B. Polymorphism of rare earth disilicides. Phys Chem. 1959;63:2073–4.
27. Kranenberg C, Johrendt D, Mewis A. Investigations about the stability range of the $CaAl_2Si_2$ Type structure in the case of ternary silicides. Z Anorg Allg Chem. 1999;625:1787–93.
28. Bobev S, Tobash PH, Fritsch V, Thompson JD, Hundley MF, Sarrao JL, Fisk Z. Ternary rare-earth alumo-silicides-single-crystal growth from Al flux, structural and physical properties. J Solid State Chem. 2005;178:2091–103.
29. Dubenko IS, Evdokimov AA, Ionov VM. Crystal structure of Tb_6Al_3Si. Sov Phys Crystallogr (Engl Transl). 1987;32:201–3.